© 2017. Published by The Company of Biologists Ltd | Journal of Experimental Biology (2017) 220, 1411-1422 doi:10.1242/jeb.145623

RESEARCH ARTICLE

Archer fish jumping prey capture: kinematics and hydrodynamics

Anna M. Shih*, Leah Mendelson* and Alexandra H. Techet‡

ABSTRACT

Smallscale archer fish, *Toxotes microlepis*, are best known for spitting jets of water to capture prey, but also hunt by jumping out of the water to heights of up to 2.5 body lengths. In this study, high-speed imaging and particle image velocimetry were used to characterize the kinematics and hydrodynamics of this jumping behavior. Jumping used a set of kinematics distinct from those of in-water feeding strikes and was segmented into three phases: (1) hovering to sight prey at the surface, (2) rapid upward thrust production and (3) gliding to the prey once out of the water. The number of propulsive tail strokes positively correlated with the height of the bait, as did the peak body velocity observed during a jump. During the gliding stage, the fish traveled ballistically; the kinetic energy when the fish left the water balanced with the change in potential energy from water exit to the maximum jump height. The ballistic estimate of the mechanical energy required to jump was comparable with the estimated mechanical energy requirements of spitting a jet with sufficient momentum to down prey and subsequently pursuing the prey in water. Particle image velocimetry showed that, in addition to the caudal fin, the wakes of the anal, pectoral and dorsal fins were of nontrivial strength, especially at the onset of thrust production. During jump initiation, these fins were used to produce as much vertical acceleration as possible given the spatial constraint of starting directly at the water's surface to aim.

KEY WORDS: Prey capture, Jumping, Archer fish, Rapid maneuvering, Particle image velocimetry

INTRODUCTION

Jumping by any organism requires substantial energy and precise muscular coordination. Aquatic jumpers in particular must produce thrust in manners compatible with the transition in fluid media and drop in density (and thus force-producing ability) between water and air. Organisms ranging in size from large marine mammals and sharks (e.g. Brunnschweiler, 2005; Davenport, 1990; Hester et al., 1963; Hui, 1989) to small copepods (Gemmell et al., 2012) have developed aquatic jumping strategies compatible with their size and survival goals (e.g. prey capture, escape, mating or migration).

Among fishes specifically there is remarkable diversity in jumping strategies. In some fish species, including trout and salmon, jumping is an oft-observed migratory behavior (e.g. Kondratieff and Myrick, 2006; Lauritzen et al., 2005, 2010), executed from depth in plunge pools at the base of waterfalls. For predator evasion, African butterfly fish (*Pantodon buchholzi*) and freshwater hatchetfish (Gasteropelecidae) jump upwards in a ballistic motion, aided by their pectoral fins in exiting the water (Saidel et al., 2004; Wiest, 1995). The Trinidadian guppy (*Poecilia reticulata*) jumps spontaneously for population dispersal in waterfall-laden environments (Soares and Bierman, 2013). The guppy's jumping behavior includes a preparatory phase of slow backward swimming using the pectoral fins, followed by forward acceleration with kinematics similar to C-start maneuvers and burst swimming.

Jumping to feed requires more precision than jumping for migration or escape (e.g. Matthes, 1977; Lowry et al., 2005; Pronko et al., 2013). For feeding strikes in general, Weihs (1973) surmised that when a fish was sufficiently motivated by hunger, efficiency was secondary to short-term energy use. Ultimately, for long-term survival purposes, the overall energetic cost of feeding by jumping should not exceed the energetic gain provided by the targeted prey. The African tetras *Brycinus nurse* and *Alestes baremoze* can jump up to 1 m into the air to dislodge seeds from rice plants and then eat the seeds after they have fallen into the water (Matthes, 1977). The mangrove rivulus (*Kryptolebias marmoratus*) uses multiple kinematic modes, including jumping S-type 'launches', to travel up banks to feed on land (Pronko et al., 2013). Lowry et al. (2005) revealed silver arawana (*Osteoglossum bicirrhosum*) jump using S-starts similar to those executed by ambush predators (e.g. Webb, 1984; Porter and Motta, 2000) after a period of burst swimming. The arawana's kinematics for aerial feeding were faster and included larger amplitude body motions than during in-water feeding.

As emphasized by Lowry et al. (2005), having more than one prey capture mode expands an organism's 'ecological niche' and gives it a 'competitive advantage' in hunting and foraging. Archer fish (genus *Toxotes*) are found in mangrove swamps, river mouths and upstream brackish and freshwater regions (Lüling, 1963; Allen, 1978). *Toxotes* spp. eat insects or small aquatic animals that live near the water's surface. Archer fish employ several hunting strategies: spitting a water jet at an aerial target such that it falls into the water to be eaten, rapidly lunging in the water for fallen prey or jumping to capture aerial prey (Bekoff and Door, 1976). This wide range of foraging behaviors makes the archer fish a model predator and a unique fish for further hydrodynamic and biological investigation.

Previous studies of archer fish hunting have used spitting, including control of jet hydrodynamics and aim, as an indicator of the fish's cognitive capabilities (e.g. Verwey, 1928; Rossel et al., 2002; Timmermans and Souren, 2004). Schlegel et al. (2006) found that archer fish fire larger masses of water as their prey grows in size (and thus attachment strength to leaves and branches) to avoid expending unnecessary energy on smaller, weaker prey. Vailati et al. (2012) proposed that archer fish modulate the flow rate of the jet over time to maximize force on prey. Experiments have also suggested that jets are focused for specific prey heights (Gerullis and Schuster, 2014) and hunting fish compensate for their distance to the prey (Burnette and Ashley-Ross, 2015). This control over spitting is facilitated by sophisticated eyesight. Despite refraction of light at the

Experimental Hydrodynamics Laboratory, Department of Mechanical Engineering, Massachusetts Institute of Technology, Cambridge, MA 02139, USA.
*These authors contributed equally to this work

‡Author for correspondence (ahtechet@mit.edu)

A.H.T., 0000-0003-3223-7400

Received 16 August 2016; Accepted 27 January 2017

Journal of Experimental Biology (2017) 220, 1411-1422 doi:10.1242/jeb.145623

surface and gravity effects on the water jet, spitting still hits prey with impressive accuracy (Dill, 1977; Timmermans and Vossen, 2000; Schuster et al., 2004). Aiming studies have shown *Toxotes* can account for viewpoint dependency (Schuster et al., 2004) and connect apparent size of the bait with relative position to the target (Schuster et al., 2006). Archer fish are also capable of pattern recognition, most dramatically exhibited by Newport et al. (2016), who successfully trained archer fish to spit at printed human faces.

Successful prey capture following spitting requires advanced rapid maneuvering capabilities (Wöhl and Schuster, 2007; Krupczynski and Schuster, 2013; Reinel and Schuster, 2014, 2016). For rapid maneuvering in water, archer fish execute C-starts, also known as escape responses when used for predator evasion, in which the body bends into a 'C' shape before straightening and accelerating (e.g. Domenici and Blake, 1997). Wöhl and Schuster (2007) found no difference between the maximum speeds of predictive feeding strikes and escape responses resulting from being startled. C-starts were reported to reach peak linear speeds above 20 body lengths s^{-1} and accelerations up to 12 times that of gravity (Wöhl and Schuster, 2007). Reinel and Schuster (2014) further found that archer fish can control speed following a C-start without performing any additional tail beats to accelerate.

Cognitively, the prey capture behaviors exhibited by archer fish are influenced by learning and competition. Rossel et al. (2002) found when prey were dislodged, archer fish used the initial trajectory to predict the direction, speed and distance at which the prey would land. Fish would then turn accordingly to pursue regardless of whether they were the shooter. Archer fish hunting is influenced by competition, and fish kept in schools have been observed to shoot more when competing for resources (Goldstein and Hall, 1990; Davis and Dill, 2012). Davis and Dill (2012) observed a high degree of kleptoparasitism in captive archer fish, with fish stealing prey shot down by another fish 43.6% of the time in captive groups of three to seven fish and an increasing probability of theft the more shots were required to bring down a particular prey. Additionally, Davis and Dill (2012) found that the frequency of jumping was greater in larger groups of fish: jumping constituted 29% of the total prey capture behaviors observed in a group of seven fish compared with 17% of behaviors in a group of three fish. Based on field recordings, Rischawy et al. (2015) suggested that competition was an evolutionary rationale for archer fish spitting, vision and predictive starts, as their habitats were also inhabited by other species of surface-feeding fish capable of fast responses to hydrodynamic stimuli such as prey hitting the water's surface.

While jumping may compromise stealth or be less successful with moving targets, it presents a self-sufficient mode of prey capture where the jumping fish is the most likely one to capture the prey. This study builds on previous knowledge of archer fish aiming and maneuvering to provide detailed characterization of the jumping specializations in these fish. Study of this behavior will ultimately enable assessment of the role of jumping as a competitive foraging strategy. High-speed video was used to analyze the kinematics and ballistic energetics of the jump. Particle image velocimetry (PIV) was used to understand the roles of the fish's fins during upward propulsion. Combined, these data expand knowledge of a relatively unmentioned aspect of the archer fish's lifestyle: aerial prey capture.

MATERIALS AND METHODS

Fish

Ten smallscale archer fish [*Toxotes microlepis* (Günther 1860)] were imported from a local aquarium store and housed in a 75% full 55 gallon (122×33×51 cm) brackish water aquarium (25–28°C, salinity 9.5 mS cm^{-1}, 9 h:15 h light:dark cycle). Because the fish were not bred in captivity, ages and sexes were unknown. Fish were fed freeze-dried brine shrimp or bloodworms at the water's surface daily. Fish were trained to jump prior to experiments by replacing daily surface feeding with food suspended from a string above the tank. During training, food was temporarily removed if the fish spat instead of jumping. Training was performed at least twice weekly for at minimum 1 month prior to testing. Five fish jumped for greater than 15 trials under the kinematic experimental conditions described in the next section. All experiment protocols were approved by the Massachusetts Institute of Technology Committee on Animal Care (protocol no. 0709-077-12).

Fish lengths and caudal fin surface areas were obtained by digitally photographing each fish in a narrow aquarium with a gridded background to provide scale and distortion correction. Images were taken with a Canon EOS 20D digital SLR camera equipped with an 18–55 mm zoom lens. Camera calibrations were verified by photographing an object of known length in the same tank. Standard length (6.8–11.1 cm range) was used as the characteristic body length (BL) scale to normalize data. The caudal fin surface area (1.7–5.3 cm^2) was proportional to the length. Fish mass (7.9–28.3 g range) was obtained by weighing a beaker of water before and after adding the fish. Physical dimensions of each specimen are presented in Table 1, along with the number of kinematic trials for each fish, the maximum height and the prey capture success rate, which was determined as the percentage of trials in which the mouth closed on the bait. Failed jumps with bait heights below the maximum successful jump height of each fish were considered for analysis, but failed jumps with bait heights above the maximum successful jump height were not. Because the focus of this study was on the height attained, successful and failed capture kinematics were analyzed together.

Kinematic analysis

Kinematic imaging was performed in the home tank. Custom plastic dividers were used to separate one fish for study while permitting it to swim freely and allowing water flow through the entire tank. A dried *Gammarus* shrimp (Tetra, Blacksburg, VA, USA) was suspended on a wire above the water's surface for a range of heights from 0.25 to 2.5 BL to elicit jumping maneuvers. Bait position within the tank sufficiently prevented hydrodynamic wall

Table 1. Standard length, tail area and mass of each fish

Specimen no.	Length (cm)	Tail area (cm^2)	Mass (g)	Jumps (all views)	Jumps (tail kinematic views)	Max. height [cm (BL)]	Success rate (%)
1	11.1	5.3	28.3	16	10	11.0 (1.0)	94
2	9.8	5.1	23.6	24	17	14.7 (1.5)	92
3	7.0	2.2	7.9	18	8	13.7 (2.0)	94
4	6.8	1.7	10.2	16	8	15.5 (2.3)	87
5	7.6	2.6	9.3	24	11	20.0 (2.6)	71

The total number of jumps, maximum observed height and success rate of each fish are also provided.

Journal of Experimental Biology

Journal of Experimental Biology (2017) 220, 1411-1422 doi:10.1242/jeb.145623

effects on the jump flow field. Jumps were recorded at 700–900 frames s^{-1} (0.0011–0.0014 s between frames) using an IDT Motion Pro X3 high-speed camera (1280×1024 pixels, 900–1008 µs exposure time). A Nikon Nikkor 50 mm lens (aperture *f*/4–5.6) yielded fields of view between 12×15 cm and 27×34 cm. The scene was back-illuminated by a bank of diffused fluorescent lights.

Kinematic image analysis was performed using MATLAB R2014a (MathWorks, Natick, MA, USA). A total of 98 jumping sequences were analyzed (16–24 per specimen). To synchronize time scales, t=0 s was defined as when the first jumping stroke was initiated by the fish's caudal fin. Positions of the snout, caudal fin, bait and free surface were digitized using the custom MATLAB software package DLTdv5 (Hedrick, 2008). The snout was tracked automatically, while all other points were digitized manually. The vertical position of the snout was smoothed using a quintic smoothing spline to ensure a continuous second derivative (Walker, 1998). Jump height (h_{max}) was defined as the maximum snout height above the free surface. Upward velocity (v) and acceleration (a) were calculated by differentiating the spline fit of the snout position. Body midline traces were determined in MATLAB by digitizing approximately 10 points from the snout to the caudal fin along the fish's centerline and fitting a cubic spline between the points. The midline spline was evaluated at every pixel along the length of the fish and converted to physical units for visualization.

Snout position was tracked to determine vertical trajectories because it had high contrast with the image background and could be easily detected for automatic tracking in the image data. Snout position also served as a better indicator of aim than center of mass (COM) position because the goal of a jump was for the fish's mouth to reach the bait. The gravitational potential energy ($E_P=mg\Delta h$), kinetic energy (E_K=0.5 mv^2) and total energy ($E=E_P+E_K$) were calculated over time for each run by assuming the COM was a fixed distance below the snout and followed a similar vertical trajectory. In the energy calculations, which treated the fish as a ballistic projectile, m was the overall mass of the fish, g=−9.8 m s^{-2} was gravitational acceleration and Δh was the change from initial to maximum snout height. Given the nature of the jump kinematics, approximating the COM position from the snout position contributed minimal error to the energy estimates. As shown in Movie 1, the snout remained aimed at the bait for the jump duration and there was not significant body bending until after bait capture. Direct tracking of a point at the stretched-straight COM in five validation runs (one per specimen) had a root mean squared error (RMSE) of 2–4% and a maximum of 8% disagreement with the estimate of COM position as a constant offset from the snout. Similarly, Tytell and Lauder (2008) found small displacement of the COM of a bluegill sunfish during the extreme bending of a C-start maneuver, and Xiong and Lauder (2014) estimated at maximum 5% error in COM tracking during forward swimming by assuming the COM was a fixed point on the fish body.

The digitized caudal fin trajectory was used to count peak-to-peak propulsive tail strokes. Strokes that ended or initiated at the body midline were considered half strokes. Stroke amplitudes and durations were measured for runs in which the kinematic images provided a ventral view of the body and complete tail kinematics could be seen without occlusion from the anal fin. The peak-to-peak amplitude of each tail stroke was measured by plotting the lateral displacement of the tail from the body axis over time; durations were measured as the interval between successive peaks in the displacement curve. Mann–Whitney U-tests (MATLAB function ranksum) with P<0.05 considered significant were used to assess differences in stroke amplitude (in BL) and duration (in s). Comparisons were made using specimens and stroke numbers with $n\geq5$ runs with visible tail trajectories. Specific factors considered were the specimen, the timing of a stroke in a jump sequence (e.g. first stroke versus third stroke) and the overall jump height.

Flow visualization

Wake features generated by a jumping archer fish were visualized using a high-speed, near-infrared implementation of 2D PIV (Raffel et al., 1998). A 10 gallon tank (51×25×31 cm) filled halfway with water from the home tank was seeded with neutrally buoyant, polyamid particles (average diameter 50 µm, density 1.03 g cm^{-3}). Illumination was provided by a Lasiris Magnum diode continuous-wave laser with a maximum output of 2 W at 810 nm. Integrated laser optics produced a 10 deg fan light sheet. The laser was mounted below the tank with the light sheet parallel to the front wall. Particles were imaged with an IDT Y-3 camera (900 frames s^{-1}; 1260×1024 pixels) equipped with a Nikon Nikkor 50 mm lens (12×10 cm field of view).

PIV was performed at bait heights of 0.5 and 1.0 BL. Bait was positioned between the front tank wall and the laser sheet. Positioning the bait 10 cm or less from the wall ensured that the fish jumped with its ventral side (as opposed to dorsal) facing the camera. A setup diagram is provided in Fig. S1. PIV analysis focused on the initial motions of the caudal, pectoral or anal fins, as alignment between the fish and the light sheet was not guaranteed at later times in a jump. DLTdv5 was used to manually digitize the trajectory of the in-plane fin (caudal or anal) in the PIV images to determine the kinematics corresponding to the observed wake structures.

PIV images were processed with LaVision DaVis 7 software (LaVision, Göttingen, Germany) using a multi-pass cross-correlation algorithm (32×32 pixel windows; 50% overlap), yielding approximately 45 vectors per body length. Velocity fields were post-processed in DaVis with median filtering, iterative interpolation to fill empty vectors and a 3×3 averaging filter. Vorticity (ω) was computed from the velocity fields using the MATLAB function curl. To measure the strength of coherent wake vortices, circulation was calculated numerically as:

$$\Gamma = \int_A \vec{\omega}\cdot\hat{n}\mathrm{d}A = \sum_{i,j}\omega_{i,j}\delta A, \quad (1)$$

where $\hat{n}$ is the normal vector of the PIV measurement plane, i and j are indices in the x and y directions, respectively, and δA=(16 pixels)^2=0.0225 cm^2 is the enclosed area between grid points. A threshold of 25–45% of the local maximum vorticity in each vortex core was used to determine the integration region over which Eqn 1 was applied (Epps and Techet, 2007). The vorticity threshold for each case was chosen as the lowest threshold at which close-proximity wake features did not merge. This calculation underestimated the circulation because vorticity below the threshold was excluded from summation. For a given vortex core, the circulation Γ_{thr}, calculated with a threshold $\frac{|\vec{\omega}_{min}|}{|\vec{\omega}_{max}|}$, was related to the true circulation Γ as:

$$\Gamma_{thr} = \left(1-\frac{|\vec{\omega}_{min}|}{|\vec{\omega}_{max}|}\right)\Gamma. \quad (2)$$

The correction factor in Eqn 2 assumed a Gaussian distribution of vorticity (Spedding et al., 2003) and was used to estimate the true strength of each vortex from the thresholded value, thus facilitating

Journal of Experimental Biology (2017) 220, 1411-1422 doi:10.1242/jeb.145623

comparison of circulations calculated with different thresholds. Circulations were smoothed over time using a local averaging filter with a neighborhood of five time steps (0.0056 s).

The orientation of propulsive jets in the wake was measured as the median direction of the top 80% of velocity vectors in the vicinity of a velocity maximum. Angles were measured relative to vertical and were used to assess jet contributions to upward versus lateral forces.

The in-plane wake kinetic energy was calculated at each time step as:

$$E_{\mathrm{K,wake}} = \int_A \frac{1}{2}\rho|V|^2 \mathrm{d}A = \frac{1}{2}\rho \sum_{i,j} |V_{i,j}|^2 \delta A, \qquad (3)$$

where $|V|$ is the in-plane velocity magnitude and ρ is the water density (1.00 g cm^{-3} for experiment temperature and salinity). The control volume for kinetic energy calculations was identified manually to include all wake structures surrounding the fish body while limiting the inclusion of ambient flow structures and noise. For consistent filtering between kinematic and hydrodynamic energy data, the in-plane kinetic energy measurement was smoothed using a quintic spline.

RESULTS

Kinematics

Jumping kinematics followed the three stage framework for in-water fast starts (Weihs, 1973; Domenici and Blake, 1997), with preparatory, propulsive and variable stages. The three phases of the jumping behavior were: (1) hovering, (2) thrust production and (3) gliding.

Before each jump, the snout was positioned at the surface to sight prey (Fig. 1A, t=0.0 ms). Alternating motions by the left and right pectoral fins and an oscillatory wave in the caudal fin provided stabilizing forces that allowed the body to remain fixed in space. The vertical position of the snout measured from the surface during hovering was −0.01±0.06 BL (mean±s.d.). Starting snout position did not vary significantly by fish (Mann–Whitney U-test, P<0.05). The body was inclined at an angle below the surface (see also Fig. S1) and the caudal fin was deflected laterally toward one side of the body (Fig. 1A, t=0–5.6 ms). At the start of the thrust production stage, the pectoral and pelvic fins abducted (Fig. 1A, t=5.6–16.8 ms) and remained abducted until exiting the water. Simultaneously, the fish initiated a series of propulsive tailbeats with an oscillatory wave traveling along the body (Fig. 1B). The snout trajectory was predominantly vertical. As more of the body left the water, the motion envelope of the tail decreased in amplitude. The thrust production phase was considered over when the fish ceased active tailbeats or completely left the water (Fig. 1A, t=56 ms). The gliding phase was when the body accelerated only due to gravity or changes in posture (Fig. 1A, t=56.0–140.0 ms). This phase was considered over when the fish reached maximum height. The mouth closed on the bait during the gliding phase of a successful jump.

Bait height (h_{bait}) and jump height (h_{max}) were strongly correlated (Fig. 2A). The maximum jump height observed was

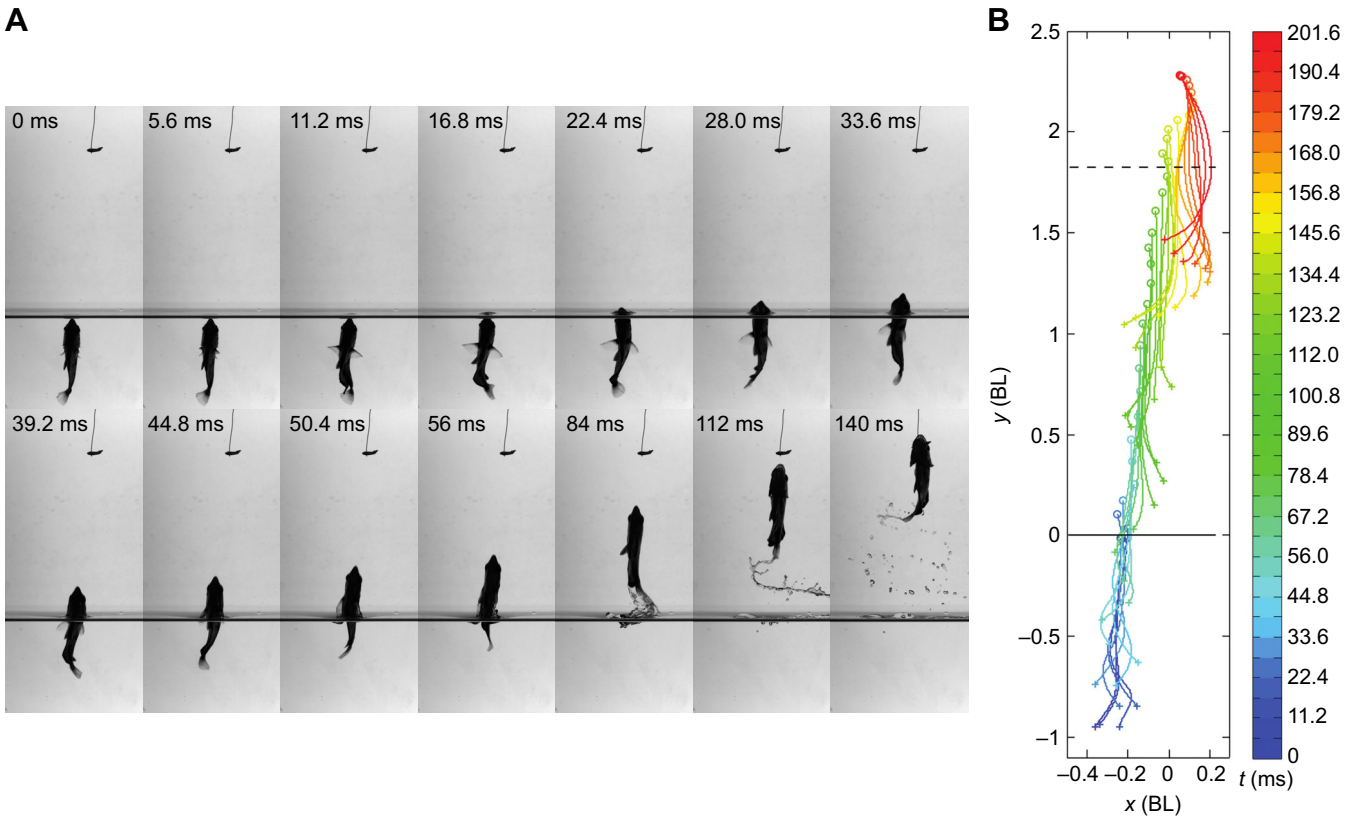

Fig. 1. Representative jumping image sequence and corresponding body midline traces of *Toxotes microlepis*. (A) Image sequence of specimen 5 jumping 2.3 body lengths (BL) above the surface. The aiming stage ended at time t=0 ms. Frames from t=5.6 to 56.0 ms showed a series of thrust-producing tailbeats. Abduction of the pectoral fins was also prominent from t=5.6 to 11.2 ms. For t>56.0 ms, the fish was above the water gliding toward the bait. Movie 1 shows video of this jumping sequence. (B) Body midline traces of the jump seen in A show traveling waves along the fish spine. The snout position is indicated by the 'o' markers and the tail position is denoted by the '+' markers. The bait height is denoted by the dotted line.

Journal of Experimental Biology

Journal of Experimental Biology (2017) 220, 1411-1422 doi:10.1242/jeb.145623

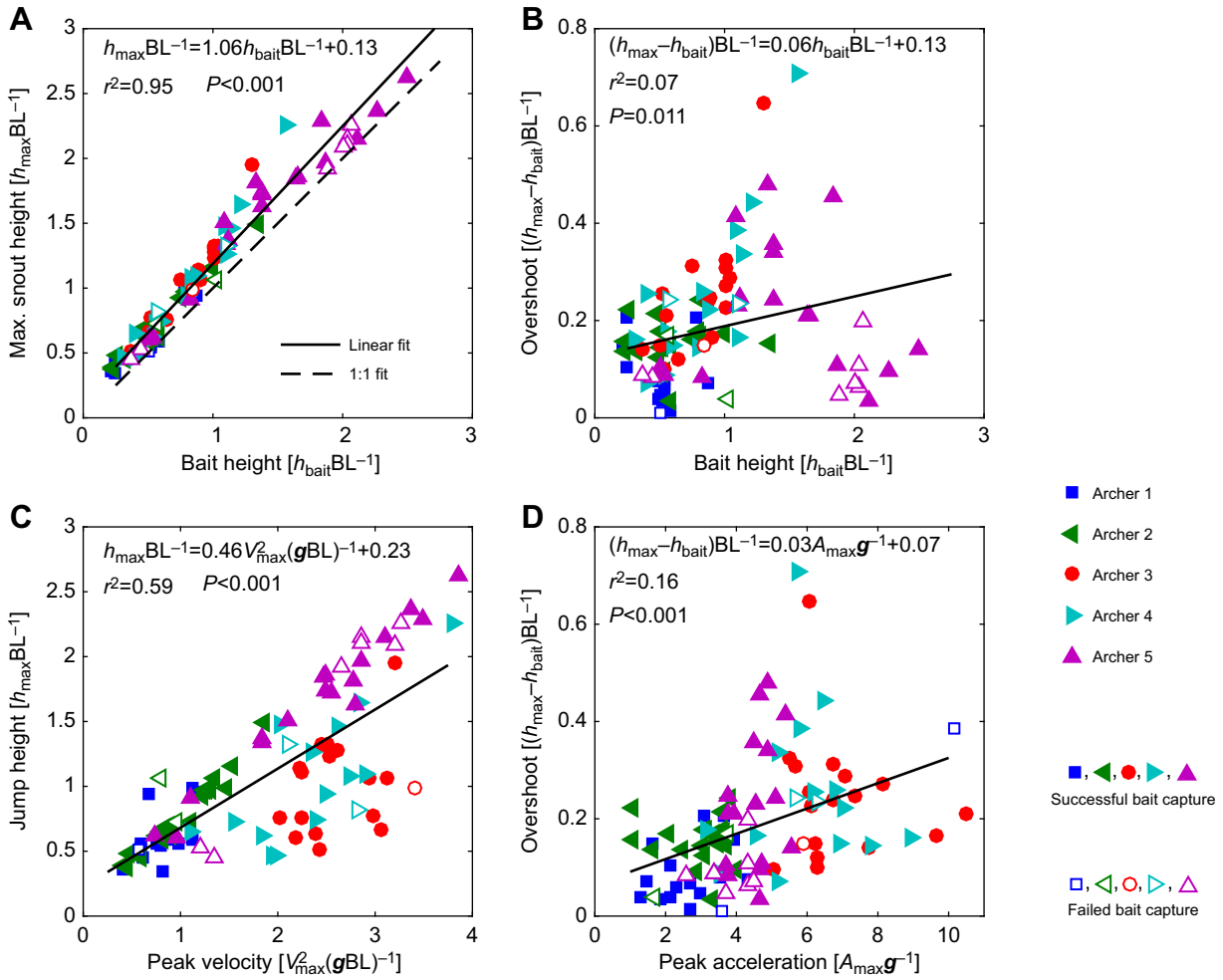

Fig. 2. Relationships between bait and jump height, bait height and overshoot, peak velocity and jump height, and peak acceleration and overshoot. All quantities are non-dimensionalized. Open markers correspond to trials where the fish does not capture the bait and closed markers correspond to trials with successful bait capture. (A) Maximum snout height was significantly correlated with bait height with a slope greater than a 1:1 relationship. (B) Overshoot, defined as jump height above the bait height, showed weak positive correlation with bait height but was greatest at intermediate bait heights. (C) Maximum velocity, non-dimensionalized by hydrodynamic Froude number $[V^2_{max}(gBL)^{-1}]$, correlated strongly with jump height. (D) Maximum acceleration, normalized by gravity, showed a positive correlation with overshoot.

approximately 2.5 BL. Jump heights above 2 BL were realized in three specimens (specimens 3–5), while the two fish of greater length and mass (specimens 1 and 2) had maximum observed jump heights of 1.0 BL and 1.5 BL, respectively. The minimum jump height observed in any of the trials was approximately 0.5 BL, though bait was positioned as low as 0.25 BL. The relationship between bait height and jump height was also quantified in terms of the overshoot (h_{max}–h_{bait}). Overshoot was weakly correlated with bait height (Fig. 2B). The median overshoot across all fish and jump heights was 0.16 BL. Variation in overshoot range between specimens was observed (Fig. S2A): specimens 1 and 2 had lower median and maximum overshoot than specimens 3–5. Undershoot, with a jump height less than the bait height, was observed during early specimen training but not during kinematic experiments.

Maximum body velocities (V_{max}) during each run ranged from 0.6 to 1.7 m s^{-1} with peak accelerations (A_{max}) from 10 to 103 m s^{-2}. The hydrodynamic Froude number $[V^2_{max}(gBL)^{-1}]$ was derived from peak velocity to normalize for size effects and correlated strongly with jump height (Fig. 2C). Acceleration, normalized by gravity, was strongly correlated with overshoot (Fig. 2D): higher accelerations were correlated with greater overshoot. Peak acceleration varied among individual fish: two of the fish (specimens 3 and 4) typically achieved higher accelerations than the others across all jump heights (Fig. S2B).

Fish executed more peak-to-peak tail strokes (n_{TB}) to jump higher (Fig. 3A). Tail strokes were not uniform; amplitudes (A_{TB}) varied across specimens and stroke number (Fig. 3B–D, Fig. S3). For specimens 2 and 3, the third stroke was significantly narrower than the first two tail strokes. In the case of specimen 5, there was a significant decrease in amplitude between strokes 5 and 6 and earlier tail strokes (Fig. 3B–D). Stroke duration differed between specimens, with specimens 1 and 2 having slower tail strokes than specimens 3–5, possibly because of their larger caudal fins. Durations were similar between all strokes by a single specimen (Fig. S3).

Time profiles of position, velocity, acceleration and energies (Fig. 4) highlighted three key times in the jump: t_{glide}, when the tail left the water completely; t_{bait}, when the snout reached the bait height; and t_{max}, when the snout reached maximum height. Peak velocity and thus ballistic kinetic energy always occurred while the tail was still in the water and before the fish reached its prey. Acceleration was

Journal of Experimental Biology (2017) 220, 1411-1422 doi:10.1242/jeb.145623

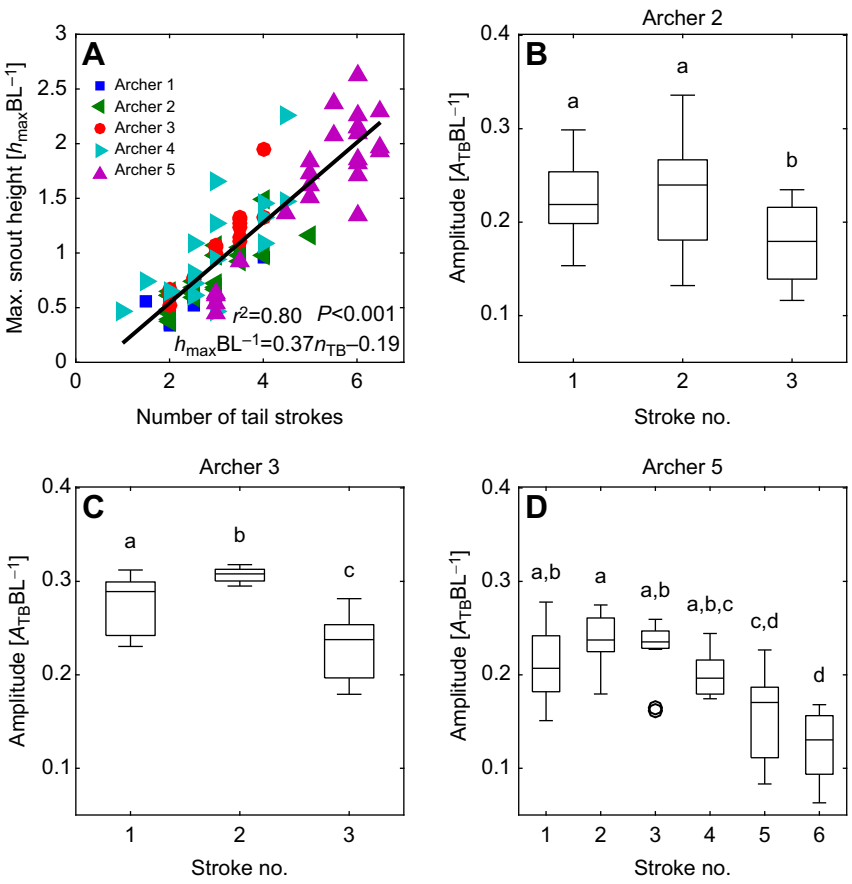

Fig. 3. Tail kinematics over increasing jump height and over the course of a single jump. (A) The number of peak-to-peak tail strokes executed by the fish increased linearly with jump height (in BL) with significant correlation (P<0.001). (B–D) Variation of amplitude (normalized by BL) with stroke number for specimens 2 (B), 3 (C) and 5 (D). Specimens 1 and 4 were excluded because of an insufficient number of runs showing full tail kinematics for greater than two tail strokes. Box plots show the median, upper and lower quartiles and whiskers to within three interquartile ranges of the upper and lower quartiles. Circles denote outliers beyond this range. Lowercase letters above boxes denote statistically distinct groups within each specimen (P<0.05) using Mann–Whitney U-tests. Data were compared within but not between specimens. Additional tail kinematic statistics are shown in Fig. S3.

greatest at jump onset. After the fish completely left the water and again after bait capture, continued tail oscillations (see Movie 1) caused changes in body posture reflected in the velocity, acceleration and energy traces; the magnitude of these fluctuations was small compared with the changes in velocity, acceleration and energy during thrust production. Despite fluctuations, the mean acceleration between t_{glide} and t_{bait} was −11.6 m s^{-2}, close to gravitational. Kinetic energy reached zero at the maximum height. Aside from the

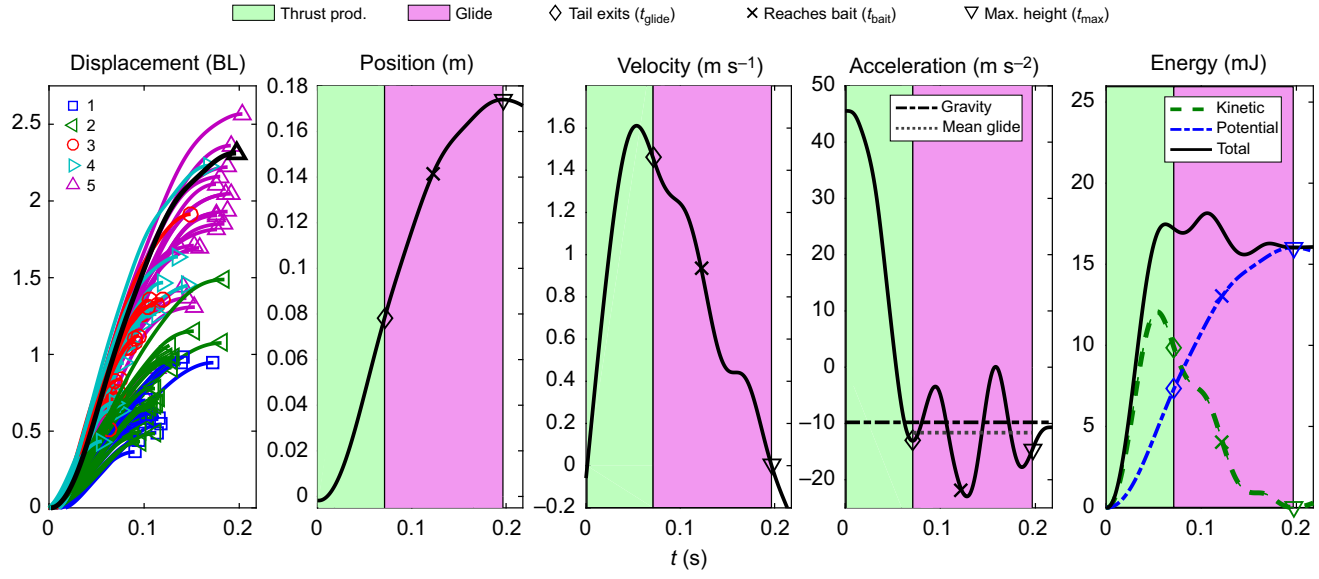

Fig. 4. Displacements for all trials and position, velocities, accelerations and energies for the 2.3 BL jump from Fig. 1. (A) Representative vertical trajectory from specimen 5 (thick black line) compared with displacement trajectories (relative to initial position) for all specimens (numeric legend) and jump heights. (B) Vertical position relative to the surface increased during thrust production and glide stages. (C) Velocity reached a maximum shortly before the tail left the water and the thrust production stage ended. (D) Acceleration was greatest at jump onset. The black dashed line shows gravitational acceleration and the grey dotted line shows the mean acceleration during the glide stage. (D) Kinetic, potential and total energy. Kinetic energy was greatest immediately before the tail left the water. The total energy increases during thrust production and plateaus during the glide stage.

Journal of Experimental Biology

Journal of Experimental Biology (2017) 220, 1411-1422 doi:10.1242/jeb.145623

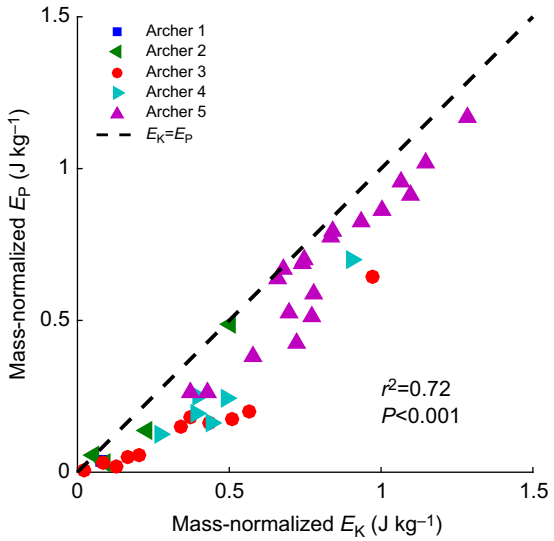

Fig. 5. Energy comparison during the glide stage. (A) Kinetic (E_K) and potential energy (E_P) balance during the glide stage for jump heights above 1 BL. Kinetic energy was calculated at t_{glide}; potential energy was measured as the change in height between t_{glide} and t_{max}. The dotted line denotes conservation of kinetic and potential energy. Energies were scaled by the mass of the fish for comparison across specimens.

aforementioned posture oscillations, the total ballistic energy plateaued during the glide stage.

Energy balance was assessed during the glide stage for jumps greater than 1.0 BL. During thrust production and for jumps in which the body was partially submerged at bait capture, hydrodynamic energy and the kinetic energies of individual fins would need to be considered along with the ballistic energies measured in this study. Maximum ballistic kinetic energies calculated during each jump ranged from 2.6 to 25.3 mJ. Changes in gravitational potential energy ranged from 2.8 to 33.7 mJ. During the glide stage, the kinetic energy when the caudal fin departed the water at t_{glide} balanced the change in gravitational potential energy from t_{glide} to t_{max} (Fig. 5).

Hydrodynamics

PIV revealed the wake structures produced by the fish during thrust production. The caudal fin and body wake during the first three tail strokes of a 1.0 BL jump consisted of coherent vortex structures shed by the caudal fin and jets initiated by the body wave between the pectoral fins and the caudal peduncle (Fig. 6). The caudal fin wake resembled the classic reverse Kármán street of forward fish locomotion with a single vortex core shed per peak-to-peak tail stroke. The first two tail strokes produced a strong vortex pair between t=0.007 and 0.023 s. At t=0.030 s, multiple positive vortex cores were observed: one from the caudal fin and one from the dorsal fin, which raw images showed was also present in the light sheet at this time (see Movie 2). A patch of negative vorticity between the two caudal fin vortices appeared to pinch off from the negative vortex core of the second tail stroke.

The appearance of wake structures from fins other than the tail (Fig. 6, t=0.030 s) and simultaneous motion of median and paired fins at the onset of a jump (Fig. 1A) motivated PIV focused on locations beyond the caudal fin. The wakes of the pectoral and anal fins for a 0.5 BL jump are seen in Fig. 7. Propulsive jets of downward orientation (±15–18 deg from vertical) appeared near both pectoral fins at t=0.010 s. The pectoral fin vortex pair on the viewer's left side advected out of the measurement plane by t=0.038 s, while the pair on the viewer's right side remained in-plane. The anal fin also shed a vortex pair with a predominantly lateral jet (76–80 deg from vertical). The same wake structures were observed for PIV performed on specimen 4 at the same jump height (see Fig. S4).

Energy transfer between the archer fish and the water was assessed quantitatively through the circulation of individual wake vortices and the total in-plane kinetic energy over time (Fig. 8). The in-plane kinetic energy was a lower bound on energy expenditure because dissipation and fluxes out of the measurement plane reduced the cumulative strength of early features at later times. Analysis considered the wake strengths of the anal and pectoral fins for a 0.5 BL jump (Fig. 7) and the caudal fin during 1.0 BL (Fig. 6) and 0.5 BL (Fig. S5) jumps, all by specimen 5. Kinematic parameters for the jumps are provided in Table S1.

The in-plane kinetic energy for the 1.0 BL jump reached a maximum at t=0.030 s, which corresponded to when three tail stroke vortices and one dorsal fin vortex were seen in the wake (Fig. 8A). The in-plane kinetic energy of the 0.5 BL case was greatest at t=0.037 s, which corresponded to the third and final tail stroke before prey capture. Although kinematic data showed that the acceleration was greatest at jump onset, the mechanical energy input during a jump was not as instantaneous.

PIV performed looking at the anal and pectoral fins had two energy peaks: one at t=0.020 s, when the first jumping motions by the anal fin and pectoral fins were completed, and one that remained relatively constant from t=0.040 s to t=0.050 s, after the second anal fin stroke had been completed. By t=0.060 s, the in-plane kinetic energy had dropped considerably, as the pectoral fin and anal fin vortices had advected out of the measurement plane. The contribution of the pectoral fins to the total energy in this case was also underestimated because only half of the pectoral fin wake was in-plane. The initial slopes (t<0.015 s) of the two 0.5 BL energy cases were similar despite measurements being focused on different fins.

The time required for the circulation of any individual fin vortex to reach peak strength was much shorter than the time scale for the kinetic energy to reach a maximum. No single kinematic stroke contributed a majority of the kinetic energy to the wake. Circulations for the caudal fin cases (Fig. 8C,D) had additional maxima after initial shedding, likely because of 3D motion affecting vortex alignment with the light sheet or interaction with out-of-plane flow features. For the 1.0 BL jump, the circulation of the second tail stroke (Fig. 6, t=0.017–0.023 s) was the largest. This stroke has the largest amplitude and shortest duration of any stroke in the sequence (Table S1).

DISCUSSION

Use of oscillatory kinematics for jumping

Archer fish jump utilizing traveling body wave kinematics (Fig. 1B), an acceleration behavior with little kinematic similarity to their in-water C-starts. Velocities (0.6–1.7 m s^{-1}) and accelerations (10–103 m s^{-2}) measured in the present study were comparable with those reported by Wöhl and Schuster (2007) for C-start maneuvers by *Toxotes jaculatrix*, a closely related species of similar morphology and size, in aquatic prey capture (0.45–2.10 m s^{-1}, 17–118 m s^{-2}) and escape scenarios (0.39–1.68 m s^{-1}, 20–90 m s^{-2}). If similar speeds and accelerations are achieved by two different sets of kinematics, the question is raised of why oscillatory acceleration kinematics are preferable for jumping, while C-type maneuvers are used for in-water feeding strikes. Precision

Journal of Experimental Biology (2017) 220, 1411-1422 doi:10.1242/jeb.145623

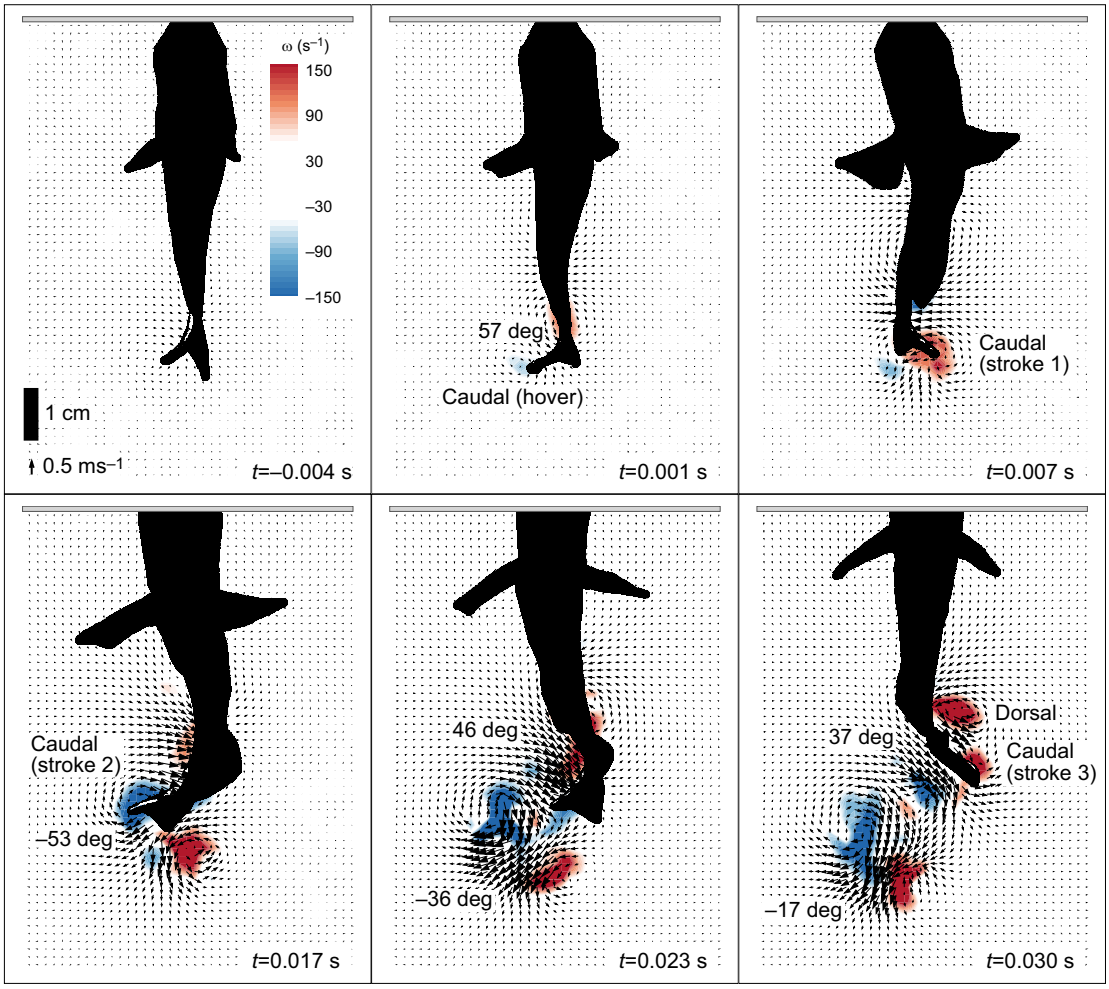

Fig. 6. Time series of particle image velocimetry (PIV) images for a 1.0 BL jump by specimen 5. Bright locations on the body mask show the position of the laser sheet. The pectoral, pelvic and anal fins were located in front of the light sheet. The grey box shows the location of the free surface. Wake structures are labeled by the direction of their propulsive jets and the fin that created them. Jet angles are relative to vertical. The caudal fin shed a vortex during each tail stroke and propulsive jets were initiated along the body in the region between the pectoral fins and the caudal peduncle. A vortex wake structure from the dorsal fin was also present in the PIV plane at *t*=0.030 s (see also Movie 2).

alone does not rationalize this difference in kinematics; archer fish perform C-starts with sufficient control over speed and orientation to pursue fallen prey by controlling the body bending speed (Wöhl and Schuster, 2007; Reinel and Schuster, 2014).

Posture and direction of motion provide some rationale for this kinematic dissimilarity. Timmermans and Souren (2004) concluded that the fish do not use their mouths to aim during spitting but angle their bodies instead. Because the mouth is not used to aim, it is therefore feasible that aiming mechanisms are not spitting-specific and can be applied to other behaviors. Jumping and predictive feeding strikes are both initiated at the surface, allowing the fish to accurately sight prey located above the water.

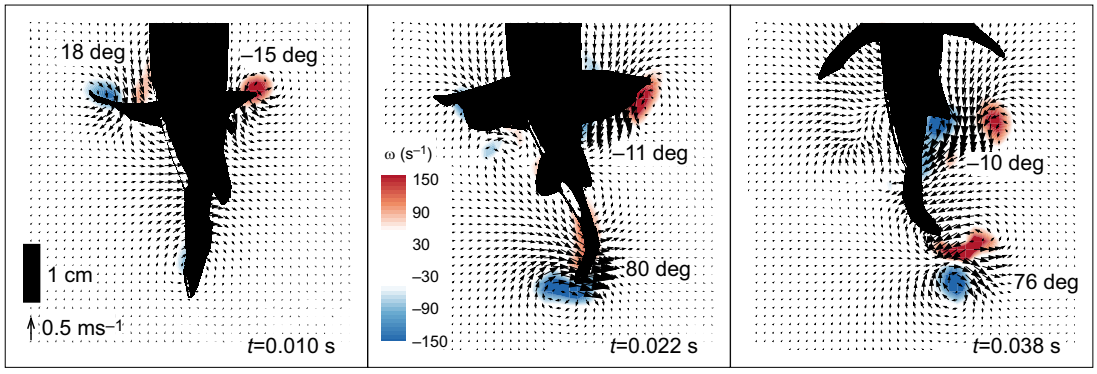

Fig. 7. PIV time series for a 0.5 BL jump by specimen 5 with the light sheet initially aligned with the anal and pectoral fins. Propulsive jets and vortices were produced by the pectoral and anal fins during jump onset. The pelvic fin was in front of the PIV plane.

Journal of Experimental Biology (2017) 220, 1411-1422 doi:10.1242/jeb.145623

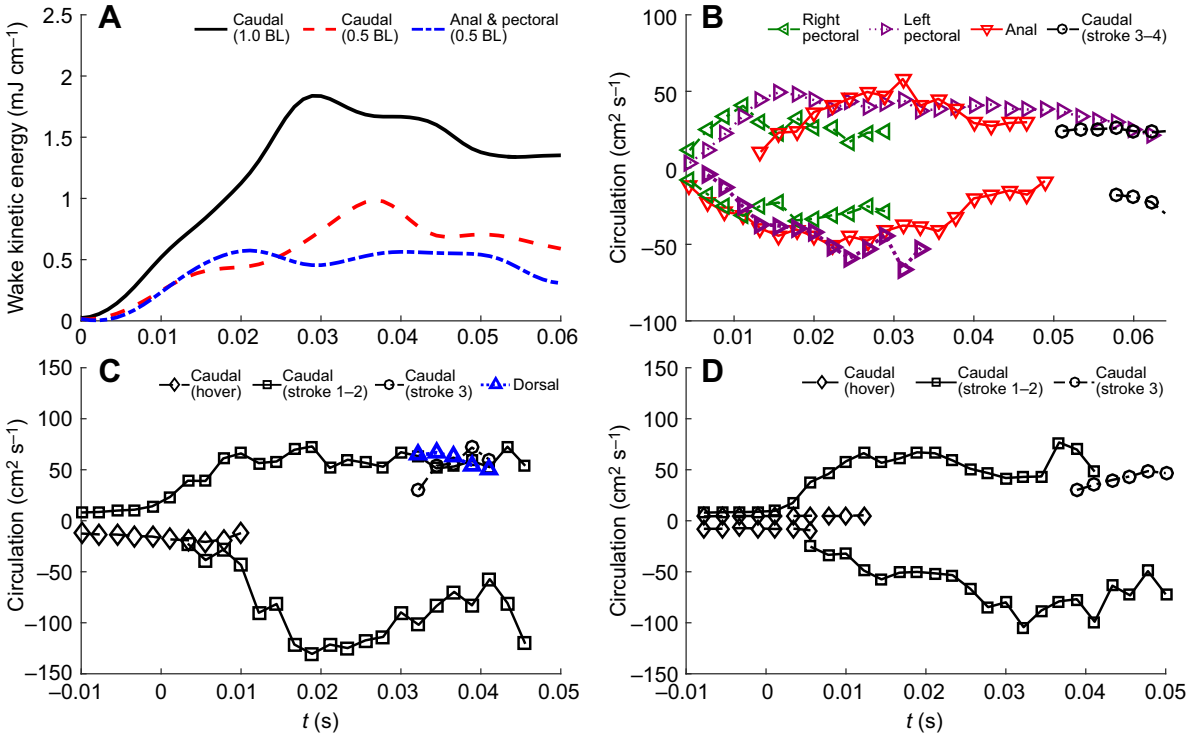

Fig. 8. Quantitative analysis of PIV data for three jumping cases by specimen 5. (A) In-plane kinetic energy for the PIV runs shown in Figs. 6, 7 and S5. (B) Circulations of vortices created by the anal and pectoral fins for a 0.5 BL jump (Fig. 7). (C) Circulations from three caudal tail strokes and the dorsal fin vortex for a 1 BL jump (Fig. 6). (D) Circulations from three caudal fin strokes of a 0.5 BL jump (Fig. S5). In B–D, markers are plotted at every other PIV time step for clarity (time between markers 0.004 s).

During a C-start, the archer fish body orientation transitions from the snout angled upward (for spitting or aiming) to level with the surface (Wöhl and Schuster, 2007), whereas during a jump the body remains pointed vertically. Body posture also varied between aerial and in-water feeding in the silver arawana. During aerial feeding, the arawana was angled upwards, compared with level with the surface during aquatic feeding (Lowry et al., 2005). However, unlike the archer fish, S-type kinematics were seen at both postures.

Despite the presence of similar aiming mechanisms for jumping and spitting, the behaviors had different overshoot patterns. Timmermans and Vossen (2000) found that spitting archer fish overshot and undershot in comparable frequency, and that specific aiming patterns varied substantially by individual. While individual variation in aim was also observed in the present study, undershoot was never observed during kinematic experiments, and specimens 3–5 had a much higher range of overshoots than specimens 1 and 2 (Fig. S2). The failure modes of spitting and jumping help explain this discrepancy. For spitting, overshoot, undershoot and poor horizontal aim all result in failed prey capture. In contrast, during jumping only undershoot or poor aim results in failure, and prey can still be captured even with substantial overshoot. For jumping, a small amount of overshoot also ensures that the mouth closes securely on the prey. In this study, the median snout overshoot (0.16 BL), the constant term (0.13 BL) in the linear relationship between bait and jump height (Fig. 2A) and the snout length of the fish (0.15–0.17 BL) were all similar in length. These results suggest that there may be an advantage to the snout traveling approximately its length beyond the bait.

Overshoot was only weakly correlated with bait height (Fig. 2B), but bait height had influence on the aiming behaviors observed in specimens 3–5. The maximum overshoots for specimens 3–5 were observed at intermediate bait heights (1–2 BL). In this range, the initial acceleration was insufficient to reach the bait but additional tail strokes may have provided more thrust than was needed. At bait heights greater than 2 BL, specimens overshot less because they were incapable of jumping higher. The two fish with the highest median and maximum overshoots (specimens 3 and 4) typically exhibited higher Froude-scaled velocities than the others (Fig. 2C). Acceleration, which was also greatest in these two fish (Fig. S2), was significantly correlated with overshoot (Fig. 2D). Specimens 3 and 4 also exhibited high initial stroke amplitudes and short initial stroke durations relative to other specimens (Fig. S3); the rapid acceleration of the tail necessary to achieve these kinematics corresponds to a large initial thrust force and likely less precise jump control.

The requirement of producing thrust even after partial water exit also influences jumping kinematics. Gazzola et al. (2012) concluded that C-starts were the optimal kinematics for traveling distances because a large volume of fluid mass accelerates with the body to create a powerful added mass force. If half of the body is airborne, the added mass force of the C-start is reduced to utilize only the submerged volume. Substantial body bending for a C-type acceleration maneuver would also put the fish into an unstable posture with the COM offset from the vertical trajectory and the snout no longer aimed directly at the bait. Oscillatory kinematics are more adaptable as the fish leaves the water. For specimens 2, 3 and 5, as the fish accelerated, the tail strokes decreased in amplitude with no significant change in duration (Fig. 3B–D, Fig. S2G–I). At jump onset, PIV showed jets formed along the body ahead of the tail (Fig. 6). As the body left the water, there was less propulsive benefit to a full body wave, as flow could only be generated by the

Journal of Experimental Biology (2017) 220, 1411-1422 doi:10.1242/jeb.145623

submerged portion. Smaller tail strokes with a reduced motion envelope could contribute thrust while minimizing wasted energy or instability above water. The initial tail stroke and simultaneous additional fin motions produced the greatest acceleration of the body, but the smaller accelerations of later tail strokes ultimately yielded the velocity and thus kinetic energy necessary to reach higher prey heights. The correlation between acceleration and overshoot (Fig. 2D) suggests that using multiple propulsive tail strokes gives the fish greater jump control and may be responsible for high prey capture success rates (Table 1). While tail strokes can be considered a discrete unit of thrust production (Fig. 3A), kinematic differences between successive strokes (e.g. amplitude and tail speed) may be responsible for the highest jumps, speeds or overshoot. The higher circulations in the caudal fin wake during a 1.0 BL jump than a 0.5 BL jump (Fig. 8) suggest this level of control may be possible, though statistical data at both jump heights are needed to confirm.

The unique vision capabilities of the archer fish, which create the constraint of jumping from the surface, have facilitated the development of a compatible jumping strategy. Archer fish exhibit a unique set of behaviors among similarly sized fish: predominantly vertical jumping of multiple body lengths, considerable accuracy (>70% for all specimens in this study) and a stationary start at the surface. The Trinidadian guppy jumped vertically to comparable heights (in body lengths), but with minimal aim. The guppy also started from a depth sufficient to execute multiple C-start accelerations and transition to burst swimming before exiting the water (Soares and Bierman, 2013). The silver arawana also accelerated before aerial feeding strikes by using burst swimming followed by an S-start (Lowry et al., 2005). In both cases, fish were able to build momentum by traveling significantly farther than a body length in the water before exiting. Considering fish water exit maneuvers initiated from the surface, mangrove rivulus initiated launches with S-type kinematics, but took off at an angle closer to 45 deg to maximize horizontal distance traveled rather than height (Pronko et al., 2013). Mangrove rivulus also used S-type kinematics during aimed prey capture pounces on a simulated bank, but the body was level with the surface and traveled no further than approximately 0.5 BL (Pronko et al., 2013).

Energetic rationale for jumping

The ballistic velocities from this study were used to compare the mechanical energy requirements of spitting, jumping and in-water pursuit. Using maximal values reported by Vailati et al. (2012) (velocity 4.5 m s^{-1}, volume 0.1 cm^3, height 0.14 m) and the density of freshwater (1 g cm^{-3}), an upper bound on the ballistic kinetic energy of spitting was estimated as approximately 2 mJ per shot. A rigid-body approximation of the kinetic energy required for in-water pursuit was estimated using the velocities reported by Wöhl and Schuster (2007) at 2.5–40 mJ for a 10 g fish, similar to the jumping kinetic energy estimated in the present study (2.7–46.9 mJ). These mechanical energy estimates suggest that in-water pursuit dominates energy consumption during hunting by spitting. In competitive scenarios in which the fastest pursuit is required, mechanical estimates suggest jumping may be of energetic parity with spitting, followed by in-water pursuit. However, these rigid-body mechanical estimates of prey-capture energy requirements do not take into account the efficiency of each behavior, including energy transferred from the fish to the water. A ballistic energy balance was only applicable once the fish completely left the water (Fig. 5). The PIV kinetic energy time history (Fig. 8A) showed energy lost by the fish to wake formation occurred during the entire thrust production stage and was not dominated by the initial acceleration. Energetic wakes were also formed by the anal and pectoral fins in addition to the caudal fin.

Size effects may play a role in motivating jumping. Larger prey provide more energy to the fish upon consumption, but are also more energetically costly to hunt using spitting. Schlegel et al. (2006) found that because the adhesion strength of prey attached to leaves or branches increases with size, a larger, higher-momentum jet and more shooting attempts were needed to capture larger prey by spitting. Jumping energetic costs depend solely on the prey height, not on its size. In the present study, two larger archer fish (specimens 1 and 2) had lower peak jump height than three smaller specimens (specimens 3–5). One possible explanation is diminishing returns between the energy required to jump and the energetic gains of a particular prey. A larger sample size than that used in the present study is needed to fully characterize size effects on jumping behavior.

Fin function at jump onset

PIV showed that the wakes of the initial fin motions by the caudal fin, pectoral fins and anal fin were all of non-trivial strength. The force produced by a fin is proportional to its size, speed and the circulation of its wake. Therefore, the comparable circulations (Fig. 8B–D) between the wakes of caudal, anal and pectoral fins suggest that despite the correlation between tail strokes and jump height, the caudal fin was not the only fin contributing to the upward thrust. The energy measurements (Fig. 8A) likewise suggest these fins were partially responsible for the energetic costs of forming a coherent wake.

The functions of the anal and dorsal fins during locomotion have been widely studied, with suggested roles including thrust augmentation and stabilization (Standen and Lauder, 2005; Tytell, 2006; Tytell and Lauder, 2008; Chadwell et al., 2012; Borazjani, 2013). These fins were also found to be active during specialized behaviors such as backwards swimming (Flammang and Lauder, 2016). In a rapid-acceleration context, Tytell and Lauder (2008) found that the dorsal and anal fins contributed momentum to the three primary propulsive jets generated by the body and tail during a bluegill sunfish C-start. In the present study, the PIV measurements showed the orientation of the anal fin and caudal fin jets could differ substantially during jumping (76–80 deg from vertical for the anal fin versus 36–53 deg for caudal fin jets). This variation suggests that the anal fin may be producing independent wake structures. In measurement planes toward the front of the anal fin, the anal fin wake appeared as an isolated vortex pair and jet (Fig. 7), suggesting independent functionality. When the PIV light sheet was positioned toward the back of the fin (Fig. S5), the caudal fin's third stroke was observed to pass through the wake of the first two anal fin strokes, suggesting that the aft portion of the anal fin also provides momentum that the caudal fin utilizes during a later tail stroke. The force-producing ability of secondary fins may be limited to key times in the jumping sequence; Borazjani (2013) found that anal and dorsal fins produced less than 5% of the thrust in a C-start except for one instance right before the start of the propulsive stage. The lateral orientation of the anal fin jet also suggests a stabilization role. The body and caudal fin produced lateral force in addition to upward thrust as propulsive jets were at a non-zero angle relative to vertical; lateral forces produced by the anal fin could counteract caudal fin forces to keep the fish's snout upright.

PIV of the pectoral fins during their abduction at jump onset revealed jets acting close to vertically (10–18 deg). By momentum conservation, these wake structures indicate that the pectoral fins

contribute upward thrust. Abduction of the pectoral and pelvic fins also increases the projected area of the fish in multiple planes and, resultantly, the added mass of surrounding fluid that must accelerate with the body. Paired fin abduction may also change the moment of inertia of the fish enough to have a stabilizing role. Given the limited space the archer fish has to accelerate before leaving the water, it is likely that the rapid, simultaneous motion of paired and median fins at jump onset generates the initial spike in acceleration (Fig. 4) before the fish performs subsequent tail strokes. Pectoral fin use during jump onset differs from that of the silver arawana and Trinidadian guppy; these fish both sweep their pectoral fins back along the body to be more streamlined (Lowry et al., 2005; Soares and Bierman, 2013). The mangrove rivulus uses its pectoral fins near the ground for stabilization during water exit over sloped surfaces (Pronko et al., 2013). Fin use during jump onset may be driven by morphology as well as space; the archer fish is less elongate and streamlined than the arawana or guppy and possesses proportionally larger pectoral fins capable of moving enough fluid mass to produce non-trivial thrust.

Volumetric measurements have recently emerged as a valuable tool for studies of biological propulsion (e.g. Flammang et al., 2011; Mendelson and Techet, 2015; Bartol et al., 2016; Murphy et al., 2016). These techniques provide the ability to simultaneously analyze all fins involved during jumping. The wake measurements from PIV presented here are a 2D view of a 3D flow with substantial ambiguity about the fish wake structure. Variability of fish position within the light sheet and wake interactions between fins both limited statistical assessment of the wake strength and energy measured from 2D PIV in this study. Mendelson and Techet (2015) showed that assumptions regarding symmetry and the alignment of a wake structure with the light sheet can lead to miscalculation of the momentum in a complex 3D fish wake with interacting flow structures. Volumetric calculation of wake energy as in Bartol et al. (2016) could further be directly compared with the ballistic energy of the fish. The kinetic energy of individual fins during the thrust production stage, energy used to deform the free surface and changes in the fluid pressure field surrounding the fish must also be considered to perform complete mechanical energy accounting during a jump.

Acknowledgements
We thank the veterinary staff at the MIT Division of Comparative Medicine and Mr Ellis London at Tropic Isle Aquarium. We also thank the anonymous reviewers for their valuable contributions to this paper.

Competing interests
The authors declare no competing or financial interests.

Author contributions
A.M.S. and A.H.T. conceived the experiments. A.M.S. performed the experiments. L.M., A.M.S. and A.H.T. analyzed the data. L.M., A.M.S. and A.H.T. wrote the paper. All authors approved the final manuscript.

Funding
This research received no specific grant from any funding agency in the public, commercial or not-for-profit sectors.

Supplementary information
Supplementary information available online at
http://jeb.biologists.org/lookup/doi/10.1242/jeb.145623.supplemental

References
Allen, G. R. (1978). A review of the archer fishes (family *Toxotidae*). *Rec. West. Aust. Mus.* **6**, 355-378.
Bartol, I. K., Krueger, P. S., Jastrebsky, R. A., Williams, S. and Thompson, J. T. (2016). Volumetric flow imaging reveals the importance of vortex ring formation in squid swimming tail-first and arms-first. *J. Exp. Biol.* **219**, 392-403.
Bekoff, M. and Door, R. (1976). Predation by 'shooting' in archer fish, *Toxotes jaculatrix*: accuracy and sequences. *B. Psychonomic Soc.* **7**, 167-168.
Borazjani, I. (2013). The functional role of caudal and anal/dorsal fins during the C-start of a bluegill sunfish. *J. Exp. Biol.* **216**, 1658-1669.
Brunnschweiler, J. M. (2005). Water-escape velocities in jumping blacktip sharks. *J. R. Soc. Interface* **2**, 389-391.
Burnette, M. F. and Ashley-Ross, M. A. (2015). One shot, one kill: the forces delivered by archer fish shots to distant targets. *Zoology* **118**, 302-311.
Chadwell, B. A., Standen, E. M., Lauder, G. V. and Ashley-Ross, M. A. (2012). Median fin function during the escape response of bluegill sunfish (*Lepomis macrochirus*). II: Fin-ray curvature. *J. Exp. Biol.* **215**, 2881-2890.
Davenport, J. (1990). Observations on the locomotion of post-larval and juvenile flying fish. *J. Mar. Biol. Assoc. UK* **70**, 311-320.
Davis, B. D. and Dill, L. M. (2012). Intraspecific kleptoparasitism and counter-tactics in the archerfish (*Toxotes chatareus*). *Behaviour* **149**, 1367-1394.
Dill, L. M. (1977). Refraction and the spitting behavior of the archerfish (*Toxotes chatareus*). *Behav. Ecol. Sociobiol.* **2**, 169-184.
Domenici, P. and Blake, R. (1997). The kinematics and performance of fish fast-start swimming. *J. Exp. Biol.* **200**, 1165-1178.
Epps, B. P. and Techet, A. H. (2007). Impulse generated during unsteady maneuvering of swimming fish. *Exp. Fluids* **43**, 691-700.
Flammang, B. E. and Lauder, G. V. (2016). Functional morphology and hydrodynamics of backward swimming in bluegill sunfish, *Lepomis macrochirus*. *Zoology* **119**, 414-420.
Flammang, B. E., Lauder, G. V., Troolin, D. R. and Strand, T. E. (2011). Volumetric imaging of fish locomotion. *Biol. Lett.* **7**, 695-698.
Gazzola, M., Van Rees, W. M. and Koumoutsakos, P. (2012). C-start: optimal start of larval fish. *J. Fluid Mech.* **698**, 5-18.
Gemmell, B. J., Jiang, H., Strickler, J. R. and Buskey, E. J. (2012). Plankton reach new heights in effort to avoid predators. *Proc. R. Soc. B Biol. Sci.* **279**, 2786-2792.
Gerullis, P. and Schuster, S. (2014). Archerfish actively control the hydrodynamics of their jets. *Curr. Biol.* **24**, 2156-2160.
Goldstein, S. R. and Hall, D. (1990). Variable ratio control of the spitting response in the archer fish (*Toxotes jaculator*). *J. Comp. Psychol.* **104**, 373.
Hedrick, T. L. (2008). Software techniques for two- and three-dimensional kinematic measurements of biological and biomimetic systems. *Bioinspir. Biomim.* **3**, 034001.
Hester, F. J., Hunter, J. R. and Whitney, R. R. (1963). Jumping and spinning behavior in the spinner porpoise. *J. Mammal.* **44**, 586-588.
Hui, C. A. (1989). Surfacing behavior and ventilation in free-ranging dolphins. *J. Mammal.* **70**, 833-835.
Kondratieff, M. C. and Myrick, C. A. (2006). How high can brook trout jump? A laboratory evaluation of brook trout jumping performance. *Trans. Am. Fish. Soc.* **135**, 361-370.
Krupczynski, P. and Schuster, S. (2013). Precision of archerfish c-starts is fully temperature compensated. *J. Exp. Biol.* **216**, 3450-3460.
Lauritzen, D. V., Hertel, F. and Gordon, M. S. (2005). A kinematic examination of wild sockeye salmon jumping up natural waterfalls. *J. Fish Biol.* **67**, 1010-1020.
Lauritzen, D. V., Hertel, F. S., Jordan, L. K. and Gordon, M. S. (2010). Salmon jumping: behavior, kinematics and optimal conditions, with possible implications for fish passageway design. *Bioinspir. Biomim.* **5**, 035006.
Lowry, D., Wintzer, A. P., Matott, M. P., Whitenack, L. B., Huber, D. R., Dean, M. and Motta, P. J. (2005). Aerial and aquatic feeding in the silver arawana, *Osteoglossum bicirrhosum*. *Environ. Biol. Fish.* **73**, 453-462.
Lüling, K. H. (1963). The archer fish. *Sci. Am.* **209**, 100-109.
Matthes, H. (1977). The problem of rice-eating fish in the central Niger Delta, Mali. In Symposium on River and Floodplain Fisheries, Bujumbura (Burundi), pp. 225-252. Bujumbura: FAO/CIFA.
Mendelson, L. and Techet, A. H. (2015). Quantitative wake analysis of a freely swimming fish using 3D synthetic aperture PIV. *Exp. Fluids* **56**, 135.
Murphy, D. W., Adhikari, D., Webster, D. R. and Yen, J. (2016). Underwater flight by the planktonic sea butterfly. *J. Exp. Biol.* **219**, 535-543.
Newport, C., Wallis, G., Reshitnyk, Y. and Siebeck, U. E. (2016). Discrimination of human faces by archerfish (*Toxotes chatareus*). *Sci. Rep.* **6**, 27523.
Porter, H. T. and Motta, P. J. (2000). A comparison of prey capture behavior and kinematics in three ram feeding fishes. *Am. Zool.* **40**, 1175.
Pronko, A. J., Perlman, B. M. and Ashley-Ross, M. A. (2013). Launches, squiggles and pounces, oh my! the water–land transition in mangrove rivulus (*Kryptolebias marmoratus*). *J. Exp. Biol.* **216**, 3988-3995.
Raffel, M., Willert, C. E., Wereley, S. and Kompenhans, S. (1998). *Particle Image Velocimetry*. New York: Springer.
Reinel, C. and Schuster, S. (2014). Pre-start timing information is used to set final linear speed in a c-start manoeuvre. *J. Exp. Biol.* **217**, 2866-2875.
Reinel, C. P. and Schuster, S. (2016). Archerfish fast-start decisions can take an additional variable into account. *J. Exp. Biol.* **219**, 2844-2855.
Rischawy, I., Blum, M. and Schuster, S. (2015). Competition drives sophisticated hunting skills of archerfish in the wild. *Curr. Biol.* **25**, R595-R597.
Rossel, S., Corlija, J. and Schuster, S. (2002). Predicting three-dimensional target motion: how archer fish determine where to catch their dislodged prey. *J. Exp. Biol.* **205**, 3321-3326.

Saidel, W. M., Strain, G. F. and Fornari, S. K. (2004). Characterization of the aerial escape response of the african butterfly fish, *Pantodon buchholzi Peters*. *Environ. Biol. Fish.* **71**, 63-72.
Schlegel, T., Schmid, C. J. and Schuster, S. (2006). Archerfish shots are evolutionarily matched to prey adhesion. *Curr. Biol.* **16**, R836-R837.
Schuster, S., Rossel, S., Schmidtmann, A., Jäger, I. and Poralla, J. (2004). Archer fish learn to compensate for complex optical distortions to determine the absolute size of their aerial prey. *Curr. Biol.* **14**, 1565-1568.
Schuster, S., Wöhl, S., Griebsch, M. and Klostermeier, I. (2006). Animal cognition: how archer fish learn to down rapidly moving targets. *Curr. Biol.* **16**, 378-383.
Soares, D. and Bierman, H. S. (2013). Aerial jumping in the Trinidadian guppy (*Poecilia reticulata*). *PLoS ONE* **8**, e61617.
Spedding, G. R., Rosén, M. and Hedenström, A. (2003). A family of vortex wakes generated by a thrush nightingale in free flight in a wind tunnel over its entire natural range of flight speeds. *J. Exp. Biol.* **206**, 2313-2344.
Standen, E. M. and Lauder, G. V. (2005). Dorsal and anal fin function in bluegill sunfish *Lepomis macrochirus*: three-dimensional kinematics during propulsion and maneuvering. *J. Exp. Biol.* **208**, 2753-2763.
Timmermans, P. J. A. and Souren, P. M. (2004). Prey catching in archer fish: the role of posture and morphology in aiming behavior. *Physiol. Behav.* **81**, 101-110.
Timmermans, P. J. A. and Vossen, J. M. H. (2000). Prey catching in the archer fish: does the fish use a learned correction for refraction? *Behav. Process.* **52**, 21-34.
Tytell, E. D. (2006). Median fin function in bluegill sunfish *Lepomis macrochirus*: streamwise vortex structure during steady swimming. *J. Exp. Biol.* **209**, 1516-1534.
Tytell, E. D. and Lauder, G. V. (2008). Hydrodynamics of the escape response in bluegill sunfish, *Lepomis macrochirus*. *J. Exp. Biol.* **211**, 3359-3369.
Vailati, A., Zinnato, L. and Cerbino, R. (2012). How archer fish achieve a powerful impact: hydrodynamic instability of a pulsed jet in *Toxotes jaculatrix*. *PLoS ONE* **7**, e47867.
Verwey, J. (1928). Iets over de voedingswijze van *Toxotes* jaculator. *De Tropische Natuur* **17**, 162-166.
Walker, J. A. (1998). Estimating velocities and accelerations of animal locomotion: a simulation experiment comparing numerical differentiation algorithms. *J. Exp. Biol.* **201**, 981-995.
Webb, P. W. (1984). Form and function in fish swimming. *Sci. Am.* **251**, 58-68.
Weihs, D. (1973). The mechanism of rapid starting of slender fish. *Biorheology* **10**, 343-350.
Wiest, F. C. (1995). The specialized locomotory apparatus of the freshwater hatchetfish family *Gasteropelecidae*. *J. Zool.* **236**, 571-592.
Wöhl, S. and Schuster, S. (2007). The predictive start of hunting archer fish: a flexible and precise motor pattern performed with the kinematics of an escape C-start. *J. Exp. Biol.* **210**, 311-324.
Xiong, G. and Lauder, G. V. (2014). Center of mass motion in swimming fish: effects of speed and locomotor mode during undulatory propulsion. *Zoology* **117**, 269-281.

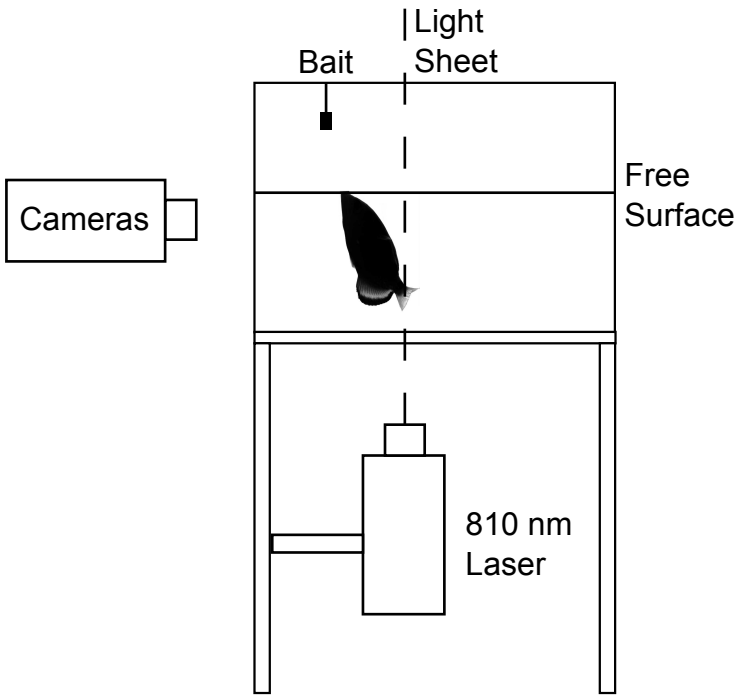

Fig. S1: **PIV experiment setup**. Two cameras running at 500 frames s^{-1} viewed the ventral side of the fish as it jumped. The laser was positioned below the tank with the light sheet parallel to the tank wall and camera image plane (into/out of the page as shown here). Bait was placed between the tank wall and the near-infrared laser sheet. The tank was partially filled to provide space for the fish to jump above the free surface.

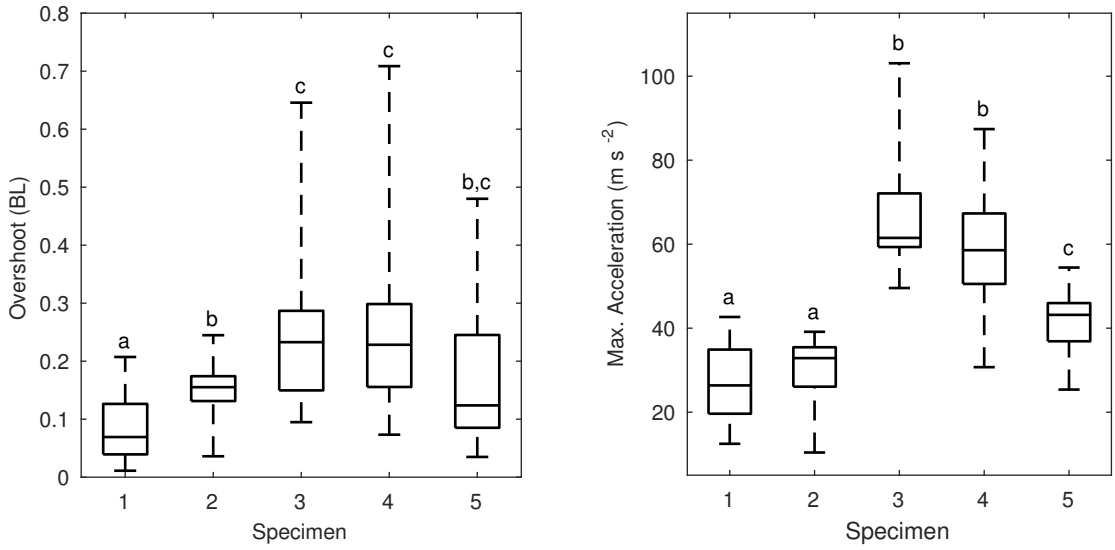

Fig. S2: **Box plots of overshoot and acceleration (for all jump heights) by specimen.** Letters (i.e., a,b,c) denote statistically significant groupings using Mann-Whitney U tests with $p < 0.05$ considered significant. (A) The two larger fish (specimens 1 and 2) exhibited lower median and maximum overshoots than the three smaller fish (specimens 3-5). (B) Acceleration varied strongly by individual specimen. Specimens 1 and 2 exhibited the lowest accelerations. Specimens 3 and 4 reached the greatest accelerations.

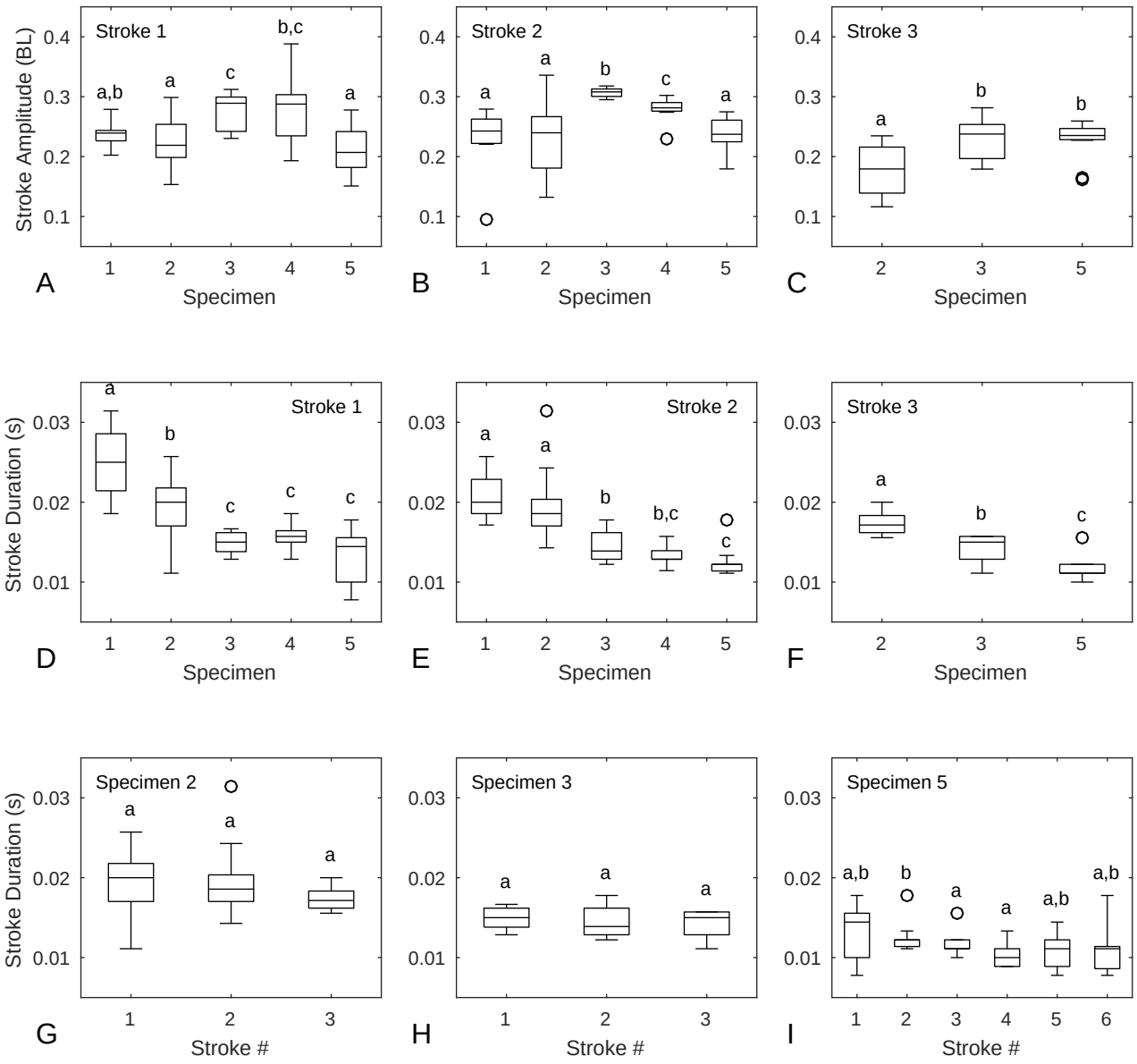

Fig. S3: **Box plots of tail amplitudes and durations.** Letters (i.e., a,b,c) denote significant differences using Mann-Whitney U tests ($p < 0.05$). Outliers (o's) are points greater than three interquartile ranges from the upper and lower quartiles. Comparisons were made for groupings with greater than five runs of available tail kinematic data. No significant differences between kinematics and the total number of tail strokes (e.g., the first stroke of a two tailbeat jump versus the first stroke of a five tailbeat jump) were observed. (A-C) Comparisons of tail stroke amplitude (normalized by BL) across specimens for the first three tail strokes. For the first two strokes, specimens 3 and 4 had the largest amplitudes, though specimen 4's first stroke was not significantly different from specimen 1's. (D-F) Stroke durations compared by specimen for the first three strokes. The two fish with the greatest lengths and tail areas (specimens 1 and 2) took the longest to complete a tail stroke. (G-I) Stroke durations compared within each specimen for all stroke numbers. Stroke durations did not vary significantly within data from specimens 2 and 3. Minimal variations were observed in stroke durations for specimen 5, though the time intervals were still very consistent between strokes.

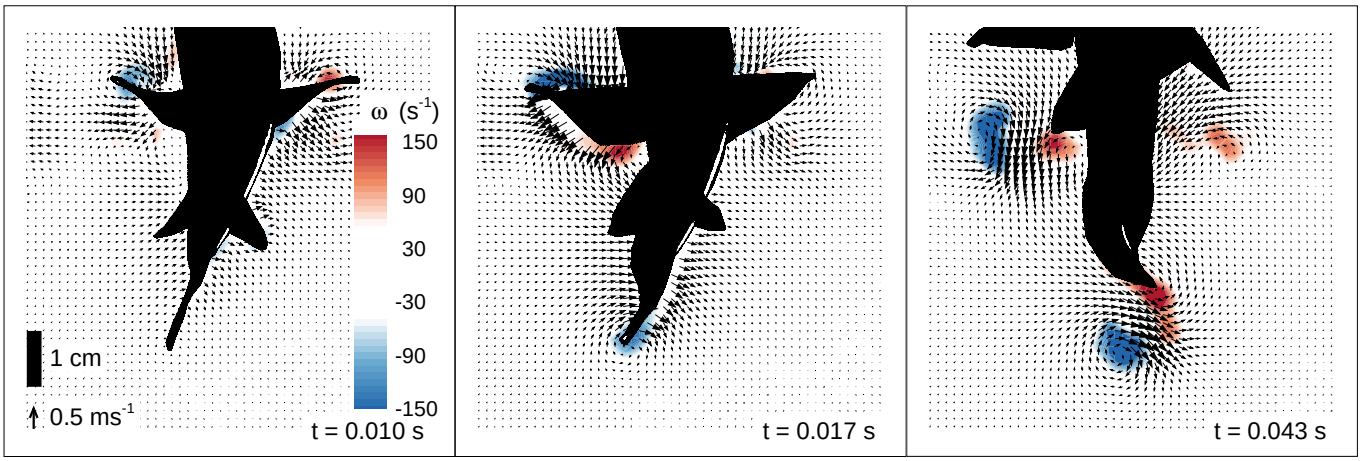

Fig. S4: **Time series of PIV images of the anal fin for a 0.5 BL jump by specimen 4.** The light sheet was positioned toward the front of the anal fin. Qualitatively, wake structures were the same as those seen in Fig. 7, with propulsive jets originating on the pectoral and anal fins.

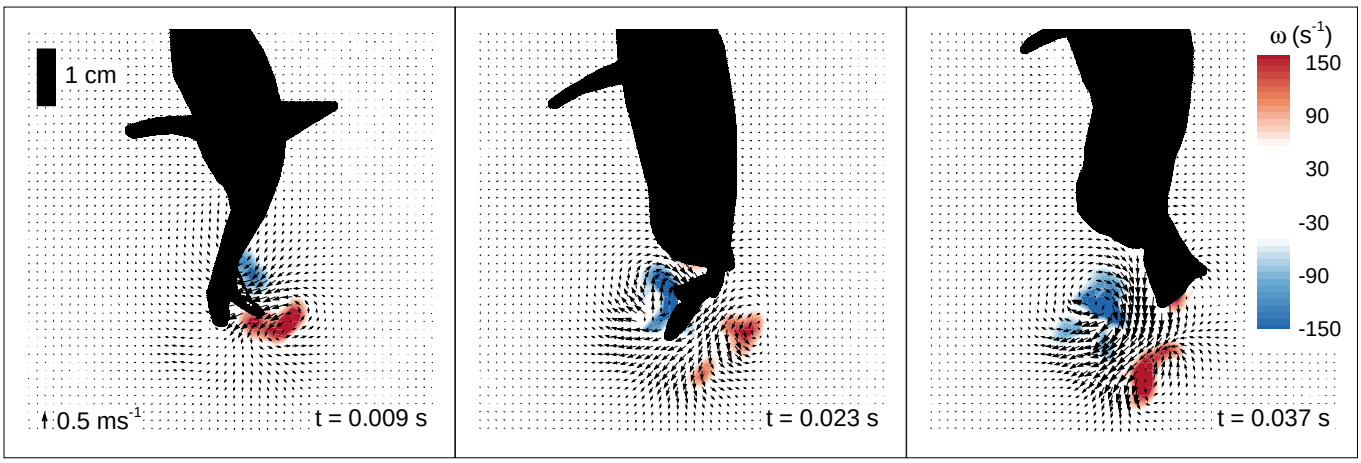

Fig. S5: **Time series of PIV images of the caudal fin for a 0.5 BL jump by specimen 5.** The caudal fin wake resembled the reverse K´arm´an street of forward locomotion. The fish executed three propulsive tail strokes before reaching the bait.

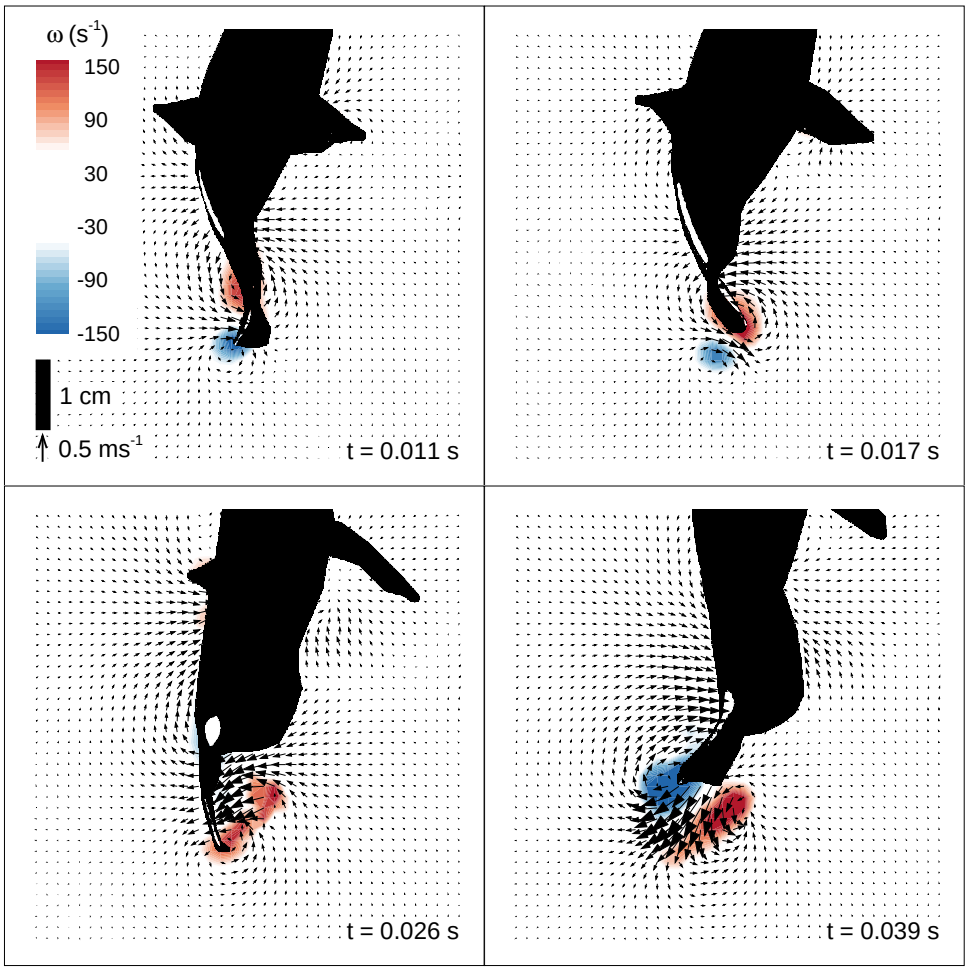

Fig. S6: **Time series of PIV images of the anal fin for a 0.5 BL jump by specimen 5.** The light sheet was initially positioned toward the back of the anal fin. At t = 0.026 s the caudal fin was observed to enter the measurement plane and interacted with the anal fin wake.

Table S1: **Kinematic and vortex parameters for PIV runs imaging the caudal fin for 0.5 BL (Fig. S5) and 1.0 BL (Fig. 6) jump heights and the anal fin for an 0.5 BL jump (Fig. 7).** Some strokes were captured in kinematics but not in PIV due to their position in the light sheet. The time to peak circulation (Γ_{max}) was measured from t = 0 s (first jumping caudal fin motion). For the 1.0 BL jump, the first tail stroke took over twice as long as the following three and was smaller in amplitude than the following three strokes. The second stroke had the shortest duration and the highest circulation. For the 0.5 BL jump imaging the caudal fin, the first two strokes had comparable amplitude and duration while the third stroke was lower amplitude and produced a weaker vortex. For the two 0.5 BL cases, the wake structures reached maximum strength over similar time intervals (0.019-0.022 s for the first vortex core and 0.031-0.032 s for the second vortex core).

Height [BL]	Fin	Stroke No.	Amplitude [BL]	Duration [s]	Γ_{max} [cm^2s^{-1}]	Time to Γ_{max} [s]
1.0	Caudal	1	0.15	0.026	73	0.019
1.0	Caudal	2	0.21	0.010	-131	0.019
1.0	Caudal	3	0.21	0.013	72	0.039
1.0	Caudal	4	0.20	0.011	–	–
0.5	Caudal	1	0.23	0.013	67	0.019
0.5	Caudal	2	0.24	0.013	-104	0.032
0.5	Caudal	3	0.09	0.015	48	0.048
0.5	Anal	1	0.16	0.018	-51	0.022
0.5	Anal	2	0.14	0.022	58	0.031

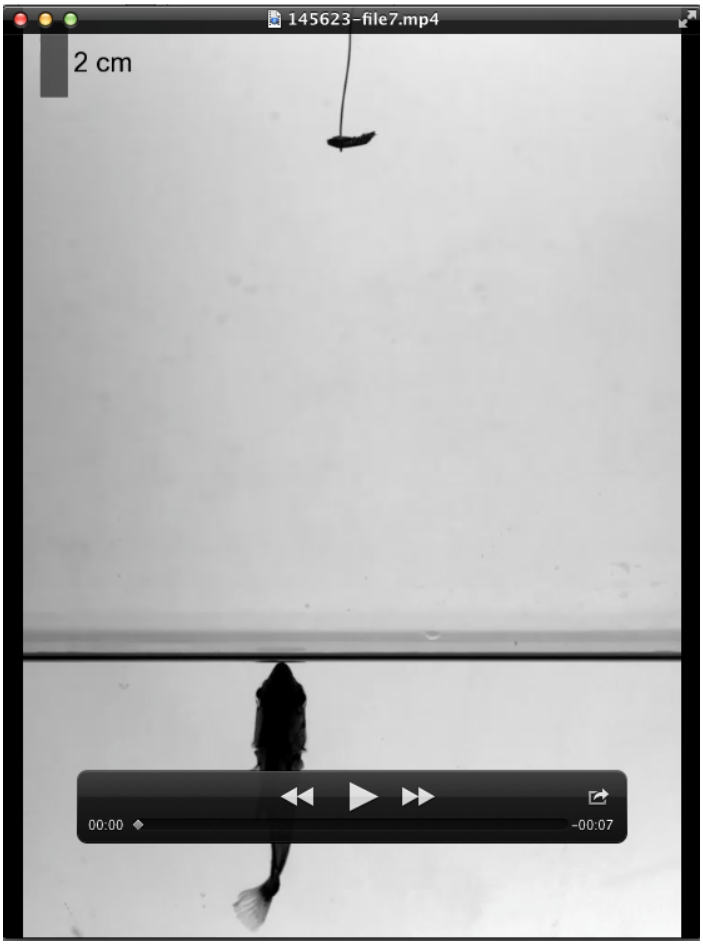

Movie 1: **2.3 BL jump by specimen 5.** This movie was recorded at 900 frames s^{-1} and played back at 30 frames s^{-1}. The fish transitions from pectoral fin hovering to jumping behaviors, executes multiple propulsive tail strokes and glides once out of the water. The movie is the same jump for which image stills and body midline traces are available in the main text (Fig. 1).

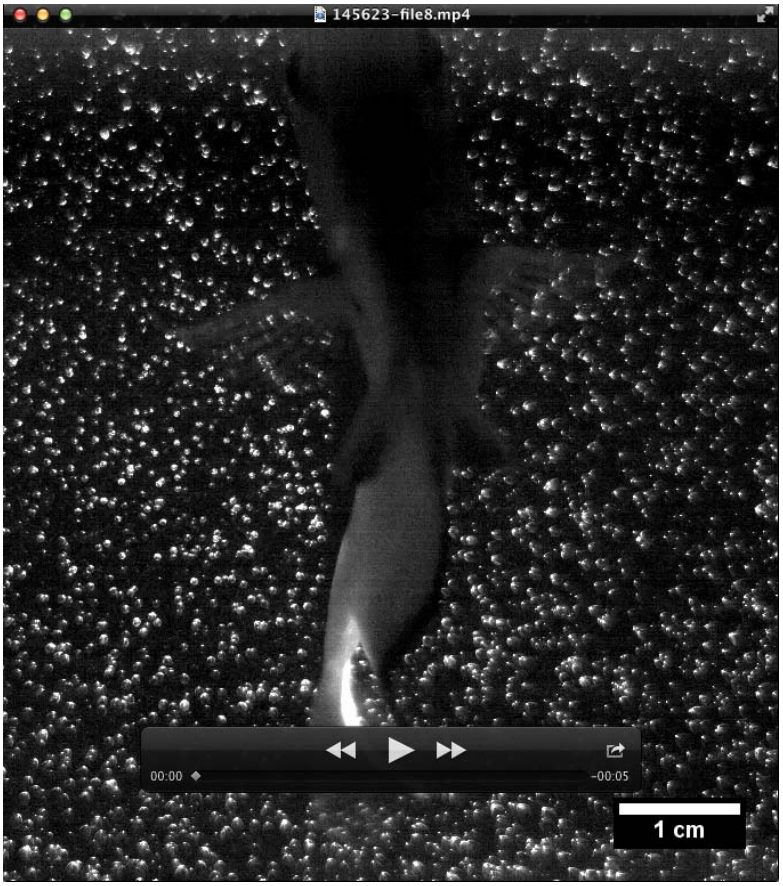

Movie 2: **Dorsal fin position during 1 BL PIV.** This movie was recorded at 500 frames s^{-1} and played back at 5 frames s^{-1}. This sequence of images shows the presence of the dorsal fin, along with the caudal fin, in the PIV light sheet (see also t = 0.030 s of Fig. 6). Contrast in the video has been linearly stretched until 2.5% of the original pixels reach saturation to increase body visibility.